Applied Catalysis B: Environmental 182 (2016) 598–610

Contents lists available at ScienceDirect

Applied Catalysis B: Environmental

journal homepage: www.elsevier.com/locate/apcatb

Catalytic total oxidation of 1,2-dichloroethane over VO_x/CeO_2 catalysts: Further insights *via* isotopic tracer techniques

Qiguang Dai[a,*], Li-Li Yin[b], Shuxing Bai[a], Wei Wang[a], Xingyi Wang[a], Xue-Qing Gong[b,**], Guanzhong Lu[a]

[a] *Key Laboratory for Advanced Materials, Research Institute of Industrial Catalysis, East China University of Science and Technology, Shanghai 200237, PR China*

[b] *Key Laboratory for Advanced Materials, Centre for Computational Chemistry and Research Institute of Industrial Catalysis, East China University of Science and Technology, Shanghai 200237, PR China*

ARTICLE INFO

Article history:
Received 29 July 2015
Received in revised form
10 September 2015
Accepted 7 October 2015
Available online 22 October 2015

Keywords:
CVOCs
Catalytic combustion
Surface hydroxyl group
Oxygen species
Isotopic tracer
Density Functional theory
Selective poisoning

ABSTRACT

Catalytic total oxidation of 1,2-dichloroethane (DCE) on CeO_2 and VO_x/CeO_2 catalysts is investigated *via* various isotopic tracer techniques, including kinetic isotope effect (KIEs) measurements, *in situ* diffuse reflection infrared Fourier transform spectroscopy (DRIFT) of deuterated 1,2-dichloroethane oxidation, H/D exchange of surface hydroxyl groups, temperature-programmed isotopic exchange (TPIE) and $^{18}O_2$ isotope labeling experiments. The activation and dissociation of C—Cl bonds is determined to be the first step of DCE oxidation, and oxygen vacancies are identified as the main active sites by KIEs and density functional theory (DFT) calculations. For VO_x/CeO_2 catalysts, surface lattice oxygen is found to directly involve in oxidation of DCE *via* the formation of intermediate species of partial oxidation such as aldehyde species or CO, which are then totally oxidized into CO_2 by the surface peroxide species. The occurrence of HCl is attributed to the reaction of surface hydroxyl groups with the dissociated Cl adsorbed on oxygen vacancies, whereas the rapid replenishment of the consumed OH is crucial for maintaining a better stability.

1. Introduction

Chlorinated volatile organic compounds (CVOCs), such as 1,2-dichloroethane (DCE), dichloromethane (DCM), trichloroethylene (TCE) and chlorobenzene (CB), are widely used in industrial processes as raw materials or solvents. However, those compounds are usually released directly into the atmosphere and recognized to be hazardous to the environment and public health. So, developing effective methods for safe disposal or/and conversion of these harmful compounds to more environment-friendly substances has become an important challenge. Among all possible approaches, catalytic oxidation or combustion is considered as one of the most promising candidates due to its low operating temperature, high activity/selectivity and high efficiency to the dilute contaminant (<1000 ppm).

In the last few years, supported VO_x [1–3], modified zeolite [4–7] and CeO_2 based [2,8–14] catalysts have gained much more attention and been regarded to be potential for industrial application due to high activity and stability. In particular, CeO_2 based catalysts, including bulk CeO_2 [8], transition metals doped CeO_2 mixed oxides [9–12], CeO_2 modified zeolites [4–7] and CeO_2 supported RuO_2 [13,14], showed promising results in the catalytic oxidation of various CVOCs. However, bulk CeO_2 as singular active component was greatly limited due to the rapid deactivation from chlorine poisoning, hence CeO_2 was often used as co-catalyst or promoter. For example, for transition metals doped CeO_2 and CeO_2 supported noble metals catalysts, the help of transition/noble metals to improve the resistance to chlorine poisoning was crucial, while the main role of CeO_2 in CeO_2 modified zeolite catalysts was the removal of coke formed on acid sites. Unfortunately, the reaction temperature maintaining stable CVOCs conversion over these catalysts was still higher than the complete oxidation temperature over bulk CeO_2 catalyst. In our recent work, VO_x/CeO_2 catalysts for catalytic oxidation of DCE were reported, and it demonstrated a high catalytic activity and outstanding stability at low temperature, more importantly, chlorinated by-products such as vinyl chloride (VC) or polychlorinated organic compounds were not detected [15].

* Corresponding author. Fax: +86 21 64253372.
** Corresponding author.
E-mail addresses: daiqg@ecust.edu.cn (Q. Dai), xgong@ecust.edu.cn (X.-Q. Gong).

http://dx.doi.org/10.1016/j.apcatb.2015.10.016
0926-3373/

The excellent stability was not attributed to the oxidation of the dissociatively adsorbed Cl into Cl_2 (Deacon reaction, oxidation of HCl), which was different with our previous reports about transition metals doped CeO_2 and CeO_2 supported RuO_2 catalysts [10,13,14].

Based on our previous results (VO_x/CeO_2 catalysts were characterized in detail and investigated in the DCE total oxidation, however, many problems were still not fully understood) [15], the scope of this paper is to further investigate the difference between oxidation behaviors of DCE over pure CeO_2 and VO_x/CeO_2 catalysts in an attempt to illuminate the roles of VO_x species and to obtain a deeper understanding of the reaction mechanism. Various isotopic tracer techniques, such as kinetic isotope effect (KIEs) measurements, *in situ* diffuse reflection infrared Fourier transform spectroscopy (DRIFT) of deuterated 1,2-dichloroethane oxidation, H/D exchange of surface hydroxyl groups, temperature-programmed isotopic exchange (TPIE) and $^{18}O_2$ isotope labeling experiments, were employed to determine the rate-determining step, the roles of surface hydroxyl groups and oxygen species (gaseous, surface active and lattice oxygen species). Moreover, selective poisoning of acid sites and density functional theory (DFT) calculations also were carried out for a better understanding of the possible active sites for CVOCs oxidation over CeO_2 based catalysts.

2. Experimental

2.1. Preparation of CeO_2 nanobelts and VO_x/CeO_2

CeO_2 nanobelts (S_{BET} = 86 cm^2/g) were synthesized *via* a facile aqueous-phase precipitation route under mild conditions (template-free and non-hydrothermal), and the highly dispersed 6%VO_x/CeO_2 catalyst (the real V loadings measured by ICP-AES analysis was 2.5%, and S_{BET} = 77 m^2/g) was prepared by a conventional incipient-wetness impregnation method of an aqueous solution of ammonium metavanadate (NH_4VO_3) and oxalic acid ($C_2O_4H_2$). The more detailed procedures and characterizations can be found in References [15,16].

2.2. Synthesis of HZSM-5

0.31 g of sodium chloride (NaCl), 2.5 g of polyethylene glycol 600 (PEG 600) and 5.625 g of tetrapropylammonium hydroxide (TPAOH, 25%) were added sequentially into 25 g of deionized water under vigorous stirring, followed by the addition of 0.1 g of aluminum isopropoxide (AIP). After ultrasonic treating for 15 min and stirring for 10 min, 3.27 g of tetraethyl orthosilicate (TEOS) was added to the solution quickly under stirring. After stirring for 24 h at room temperature, the resulting solution was transferred into an autoclave (50 ml) for further crystallization at 110 °C for 24 h and then 170 °C for 48 h under dynamic condition (60 rpm). Finally, the as-synthesized products were collected by filtration, dried, and calcined at 550 °C in air to remove the template. To produce HZSM-5, the obtained zeolites were ion exchanged four times in a large excess of aqueous 1 M solutions of NH_4NO_3 (1 M, L/S = 30 ml/g) at 80 °C and calcined again at 550 °C for 4 h.

2.3. Catalytic activity measurement

Catalytic oxidation of 1,2-dichloroethane and other halogenated hydrocarbons was carried out in a continuous flow micro-reactor constituted of a U-shaped quartz tube of 3 mm of inner diameter at atmospheric pressure. The reactor was filled with a quartz sand/catalyst/quartz sand sandwich structure. The sample weight for all catalysts was 200 mg (60–80 mesh), and the catalysts were treated for 2 h at 300 °C in 20%O_2/Ar (30 ml/min) to remove the CO_2 and H_2O before activity measurements. The gas stream was composed of 500 ppm of DCE and air in 50 ml/min, and the reaction was run from 100 (or 50) to 250 °C (or 300 °C) in a step mode with a 15 min plateau at each temperature investigated. The effluent gases (organic compounds) were analyzed by an on-line gas chromatograph equipped with a flame ionization detector (FID), and the quantitative analysis of CO, CO_2, Cl_2 and HCl was carried on an gas-detector (Shenzhen Penglei Technology Co., Ltd., PN-M4P).

2.4. Kinetic isotope effect (KIEs) measurement

For the measurements of the kinetic isotope effect, the same instrument and procedure with catalytic activity measurement was used, but the analysis of GC was operated at the lowest possible temperature (30 °C). Additionally, TPSR of the mixture of DCE and DDCE also was carried to verify the results from GC, and detailed steps could be found in Section 2.5.

2.5. Temperature-programmed surface reaction (TPSR)

The temperature-programmed surface reaction (TPSR) measurements were carried out under the conditions as the same as that in the catalytic activity tests in order to detect the reactants and products in effluence. First, the feeding 20%O_2/Ar stream containing 1000 ppm DCE flowed through the catalyst bed at 100 °C. After the adsorption–desorption of DCE reached an equilibrium, the catalyst bed was heated from 100 to 250 °C at 10 °C/min and maintained for 90 min, and then raised to 300 °C and held for 120 min. The evolution of the gas phase species (reactants and products) was monitored by a Hiden HPR-20 quadrupole mass spectrometer equipped with a heated quartz inlet capillary.

2.6. In situ *DRIFT studies*

2.6.1. In situ *DRIFT of deuterated 1,2-dichloroethane oxidation*

In situ diffuse reflectance infrared Fourier transform (DRIFT) spectroscopy of deuterated 1,2-dichloroethane oxidation was measured on a Nicolet Nexus 6700 spectrometer equipped with a MCT detector and high-temperature sample cell which was fitted with ZnSe windows. The DRIFT spectra obtained were collected in Kubelka–Munk unit with a resolution of 4 cm^{-1} and 64 scans. About 50 mg of catalyst was pre-treated by heating for 2 h at 400 °C in 20%O_2/Ar (30 ml/min) to remove the adsorbed CO_2 and H_2O, and then cooled to 50 °C. Next, the 20%O_2/Ar feeding stream containing 1000 ppm DDCE flowed through the catalyst for 30 min and the adsorption saturated. And then the cell was purged for 30 min to remove the gas phase species. Subsequently, the sample was heated up to 100, 200 and 300 °C, and the spectrum was recorded respectively.

2.6.2. H/D exchange of surface hydroxyl groups

H/D exchange was accomplished by passing an 20%O_2/Ar feed (30 ml/min) through a water saturator at 25 °C. This feed was then contacted with catalyst (about 50 mg) and placed in an *in situ* IR spectroscopy at different temperature. The exchange process was followed with IR spectroscopy to monitor the degree of exchange [17]. After H/D exchange of surface hydroxyl groups was completed, the oxidation of DCE (20%O_2/Ar stream containing 1000 ppm DCE) was recorded for different time at 200 and 300 °C.

2.6.3. Adsorption of pyridine and selective poisoning of acid sites

Surface acidity of catalysts was characterized by infrared spectroscopy of pyridine adsorption (Py-IR). First, the catalyst was dehydrated for 2 h at 400 °C in O_2/Ar. After dehydration, a background spectrum was recorded. And then, approximately 50 μl (excess) of pyridine was admitted into the cell at 50 °C,

subsequently the spectrum was recorded at various elevated temperatures. All spectra were recorded after cooling the sample to 50 °C. For the selective poisoning of acid sites, the dehydrated catalyst adsorbed pyridine at 50 °C and was purged by O_2/Ar for 30 min to remove the gaseous pyridine, a background spectrum was recorded. Next, DCE was admitted into the cell at 50, 100, 150 and 400 °C, and the corresponding spectrum was recorded respectively.

2.7. Temperature-programmed desorption of O_2 and H_2O (O_2-TPD and H_2O-TPD)

Before TPD tests, the catalyst (100 mg) was treated at 400 °C for 2 h in the presence of 20%O_2/Ar. The adsorption of O_2 or H_2O was performed at 100 °C or 50 °C, respectively. An Ar flow of 30 ml/min was used to remove the excess O_2 or H_2O. Finally, the O_2 or H_2O desorption was monitored using MS by increasing the temperature to 800–600 °C with a heating ramp of 10 °C/min.

2.8. Temperature-programmed isotopic exchange experiments (TPIE)

The $^{18}O/^{16}O$ isotope exchange (temperature-programmed isotopic exchange, TPIE) was used to evaluate the mobility of lattice oxygen in the oxide [18]. The catalyst (100 mg) was first heated in $^{16}O_2$ (5% $^{16}O_2$ in Ar flowing at 30 ml/min) at 400 °C for 1.5 h. The temperature was then decreased to 100 °C, and the flow of $^{16}O_2$/Ar was replaced by $^{18}O_2$/Ar at the same flow rate. After a period of 30 min, the catalyst temperature was increased to 800 °C at a rate of 10 °C/min. The composition of the output gas was monitored by a mass spectroscopy following the signals m/z = 36, 34 and 32, corresponding to $^{18}O_2$, $^{18}O^{16}O$ and $^{16}O_2$, respectively.

2.9. $^{18}O_2$ isotope labeling experiments

Isotope labeling experiments were carried in the flowing way: the catalyst (100 mg) was first pre-treated in $^{16}O_2$ (5% $^{16}O_2$ in Ar flowing at 30 ml/min) at 400 °C for 1.5 h, and then decreased to 100 °C; and the flow of $^{18}O_2$/Ar and DCE (1000 ppm) at the same flow rate was switched. After a period of 15 min, the catalyst temperature was increased to 200 °C and 300 °C in two-step at a rate of 10 °C/min. This pre-treatment procedure ensured almost complete removal of atmospheric and dissolved $^{16}O_2$. However, this temperature treatment was not enough to replace the chemisorbed $^{16}O_2$ on the catalyst [19].

2.10. Computational methods

We performed spin-polarized density functional theory calculations corrected by on-site Coulomb interaction (DFT + U) with the Vienna ab initio simulation package (VASP) [20,21]. The GGA-PW91 functional [22] was employed to describe the nonlocal exchange-correlation energy and the projector-augmented wave method (PAW) [23,24] was used at a kinetic energy cutoff of 400 eV to describe the core-electron interactions with Ce (4f, 5s, 5p, 5d, 6s), Cl (3s, 3p), O (2s, 2p), C (2s, 2p) and H (1s) shells being treated as valence electrons. In particular, to accurately describe the strong on-site Coulomb repulsion of the Ce 4f electrons, the DFT + U with U = 5 eV was applied, as suggested and widely used in previous studies [25,26].

The CeO_2(111) surface was modeled as a periodic slab with 9-atom-layer of oxide, and the vacuum between slabs was 12 Å. A 4×4 surface cell and corresponding $1 \times 1 \times 1$ k-point mesh were used in the calculations. All the calculations were converged until the Hellman-Feynman forces on each ion were less than 0.05 eV/Å^{-1} (the bottom three layers were kept fixed during slab calculations). Transition states of surface reactions were determined by the constrained optimization scheme [27]. Adsorption energies (E_{ads}) were calculated using $E_{ads} = -[E_{adsorbate/}CeO_2 - (E_{CeO_2} + E_{adsorbate})]$, where $E_{adsorbate/}CeO_2$, E_{CeO_2}, and $E_{adsorbate}$ are the calculated energies of an adsorbate on ceria, bare ceria, and an adsorbate in gas phase, respectively.

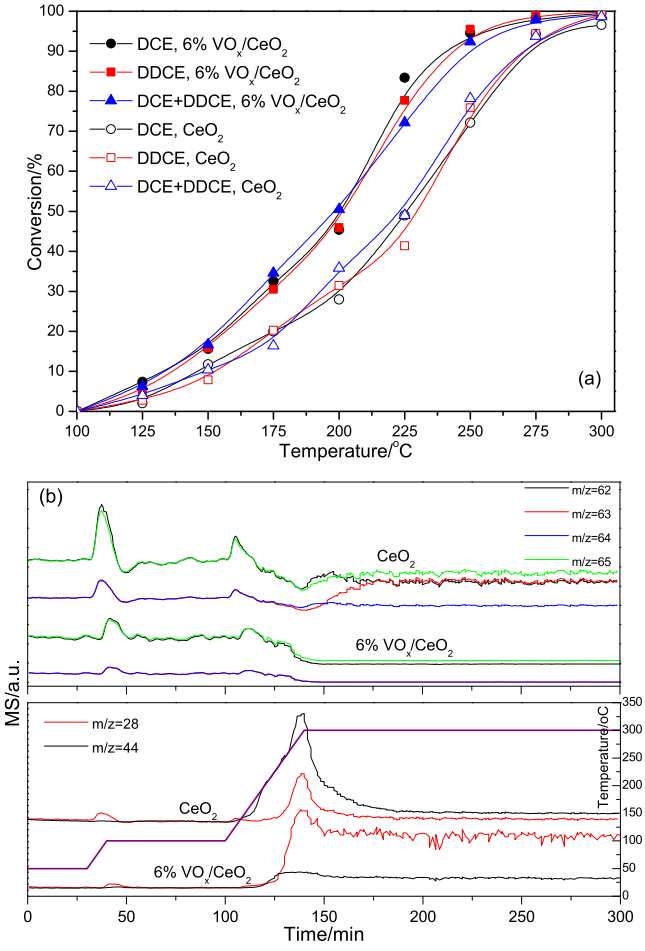

Fig. 1. The activity of CeO_2 and 6%VO_x/CeO_2 catalysts for DCE, DDCE and DCE/DDCE mixture combustion (a) and TPSR of DCE/DDCE mixture (b). Reaction conditions: 200 mg catalysts, 500 ppm DCE or DDCE, 20% O_2, Ar balance; GHSV = 15,000 h^{-1}.

3. Results and discussion

3.1. Dissociation of C—Cl bond and rate-determining step

The conversions of DCE, DDCE and DCE/DDCE mixture (molar ratio of DCE and DDCE was 1) as functions of temperature over pure CeO_2 and 6%VO_x/CeO_2 catalysts were shown in Fig. 1a. It can be clearly seen that 6%VO_x/CeO_2 showed a better activity than pure CeO_2 catalyst, which was mainly due to the inhibition effect of VO_x on the chlorine poisoning deactivation of CeO_2 [15]. Furthermore, over CeO_2 as well as 6%VO_x/CeO_2 catalyst, DCE and DDCE exhibited nearly identical light-off curves, and the effect of deuterium displacing hydrogen in DCE was negligible. Meanwhile, the kinetic isotope effect for oxidation of the DCE/DDCE mixture was found to be closed to unity (the k_H/k_D value was around (1), and the results clearly showed that the carbon-hydrogen bond activation was not a rate-determining step (RDS) in the catalytic combustion of DCE (since the activation of C—H bond was easier than C—D bond, the k_H/k_D value should be above 1 if the activation of carbon-hydrogen bond was involved in RDS), which was consistent with the reports

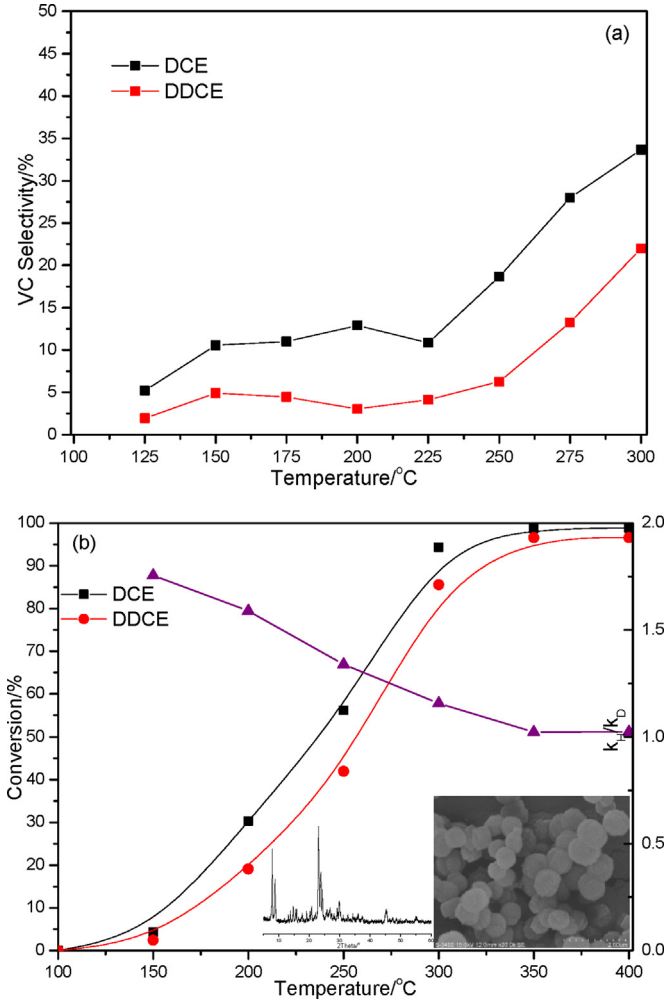

Fig. 2. Selectivity to vinyl chloride over pure CeO_2 (a), light-off curves and kinetic isotope effect of dichloroethane oxidation over HZSM-5 (b).

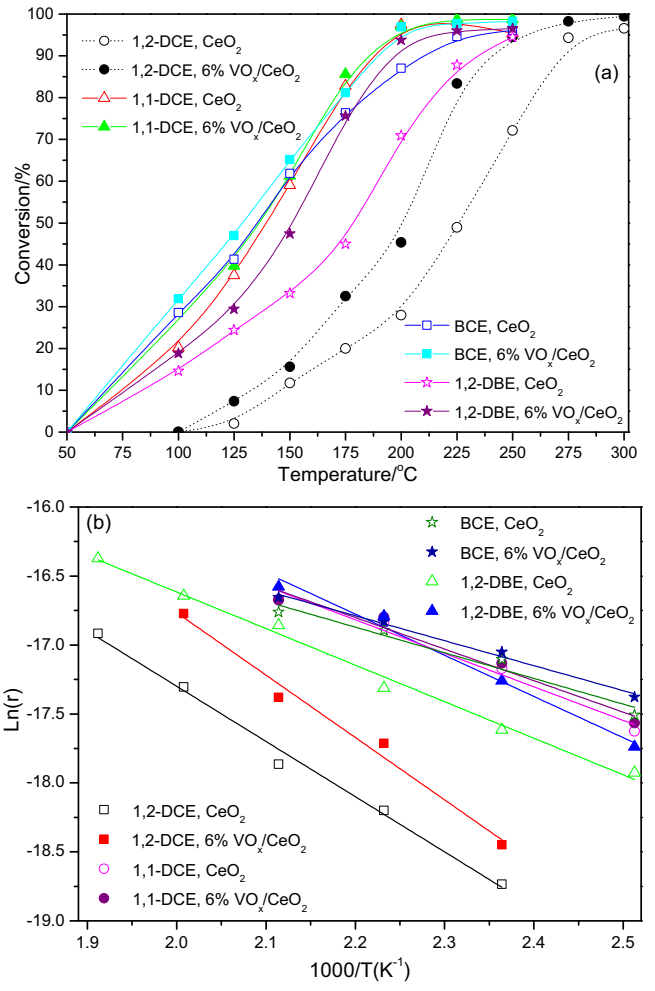

Fig. 3. Conversion curves and Arrhenius plots for the catalytic oxidation of different halogenated hydrocarbons over pure CeO_2 and 6%VO_x/CeO_2 catalysts. Reaction conditions: 200 mg catalysts, 500 ppm halogenated hydrocarbons, 20% O_2, Ar balance; GHSV = 15,000 h^{-1}.

from van den Brink et al. on catalytic combustion of chlorobenzene over Pt/γ-Al_2O_3 catalysts [28]. Additionally, our DFT results also indicated that the C—Cl cleavage of DCE was more favorable than the cleavage of C—H and CC both thermodynamically and kinetically (Fig. S1). In order to evaluate the oxidation behavior of DCE/DDCE mixture more accurately and monitor potential H/D exchange, TPSR of DCE/DDCE mixture was carried out and the results were illustrated in Fig. 1b. TPSR profiles of DCE (m/z = 62) and DDCE (m/z = 65) were largely overlapping over both CeO_2 and 6%VO_x/CeO_2, which further confirmed that the oxidation of 1,2-dichloroethane was not determined by the cleavage of C—H/C—D bonds. However, the profile of m/z = 63 presented a significant rising trend over pure CeO_2, which was an indication that some of partially deuterated vinyl chloride was formed, such as CH_2=CDCl, as the result of H/D exchange between CH_2 = CHCl and CD_2 = CDCl, DDCE or surface OD group. Our previous work had shown that vinyl chloride was a main by-product over pure CeO_2, while it was not observed over 6%VO_x/CeO_2 [15]. Additionally, CO_2 was a main product over pure CeO_2 catalyst, whereas CO was the majority over 6%VO_x/CeO_2, in consistence with our previous results [15].

Fig. 2a illustrated the selectivity to vinyl chloride (VC) of DCE and DDCE oxidation over pure CeO_2. It can be found that the the selectivity of the deuterated VC was lower than that of the hydrogenated VC, indicating that the formation of VC by-product was more difficult during the process of DDCE oxidation. It needed to be mentioned that VC is usually considered to be formed *via* the abstraction of HCl on the basic sites of CeO_2, which also involves the breaking of a C—H bond. Therefore, the observed lower selectivity of deuterated VC could be attributed to the stronger bond of C—D compared to C—H due to its extra neutron. It is well accepted in the literature that zeolites (such as HZSM-5, HY, H-MOR) have become the favorable catalysts for the decomposition of CVOCs and the abstraction of HCl (dehydrochlorination) is the first step in the reaction process [29,30], which is considered to be different from CeO_2 based catalysts. Fig. 2b presented the light-off curves and kinetic isotope effect of the DCE and DDCE oxidation over HZSM-5, which showed that the replace of hydrogen by deuterium slowed down the decomposition of DCE and the kinetic isotope effect ranged from 1.8 to 1.3 between 150 °C and 250 °C. Accordingly, the activation of C—H bond determined the abstraction of HCl and can be expected to be a RDS, by comparison, the role of C—Cl bond activation over CeO_2 based catalysts as a possible RDS was proposed.

The isotope experiments identified that the activation or dissociation of C—H bond is not a rate determining step for the catalytic combustion of DCE over CeO_2 based catalysts, but can affect the formation of by-product VC. However, the importance or role of the C—Cl bonds splitting/cleavage is still unclear. Subsequently, various halogenated ethanes, including 1,1-dichloroethane (1,1-DCE), 1,2-dibromoethane (1,2-DBE) and 1-bromo-2-chloroethane (BCE), were investigated to determine the processes of carbon-halogen bond breaking as rate-determining steps. According to Fig. 3a,

Table 1
Bond Dissociation Energies of halogenated hydrocarbons and activation energy (E_a)

Halogenated hydrocarbons	Bond dissociation energies (BDEs)/kJ/mol				Activation energy (E_a)/kJ/mol	
	C—Cl	C—Br	C—C	C—H	CeO_2	$6\%VO_x/CeO_2$
1,2-Dichloroethane	345.1[a]	–	360.6[a]	407.3[b] (384)[c]	33.3	37.6
1,1-Dichloroethane	327.9[a]	–	365.1[a]	(398[c], 391[a])	20.2	19.0
1-Bromo-2-chloroethane	315[c]	292.5[a] (262)[c]	374.0[a]	(373, 382)[c]	15.5	15.0
1,2-Dibromoethane	–	260[c]	375.7[a]	370[c]	22.0	24.8

[a] Taken from Yu-Ran Luo, Handbook of Bond Dissociation Energies in Organic Compounds, CRC Press; 1 edition (December 26, 2002).
[b] Taken from Seetula, J.A., 1998. Ab initio study of bond strengths in chlorinated ethane molecules and ethyl radicals. J. Chem. Soc. Faraday Trans. 94, 1933–1938.
[c] Calculated by L.A. Errede, Simple equations for calculating bond dissociation energies, J. Phys. Chem., 64 (1960) 1031–1034.

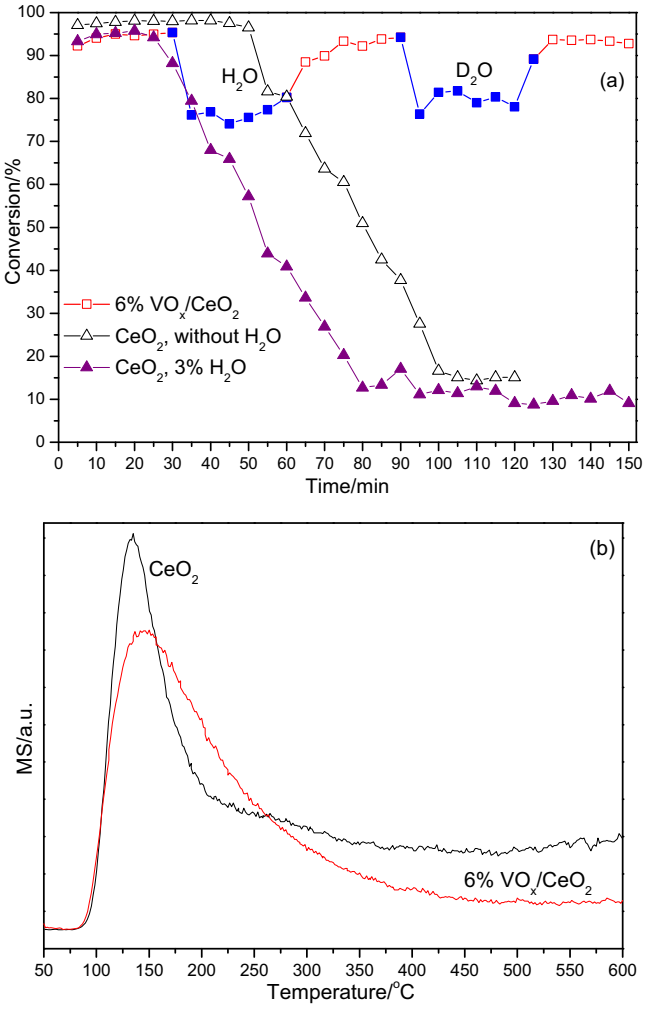

Fig. 4. DCE conversion over pure CeO_2 and $6\%VO_x/CeO_2$ catalysts at 250 °C under dry and humid conditions (a) and H_2O-TPD profiles (b). Reaction conditions: 200 mg catalysts, 500 ppm DCE, 3% H_2O vapor, 20% O_2, Ar balance; GHSV = 15,000 h^{-1}.

the conversion over CeO_2 and $6\%VO_x/CeO_2$ catalysts followed the order: 1,2-DCE < 1,2-DBE < 1,1-DCE≈BCE. Moreover, Arrhenius plots were obtained with the catalytic data in the low conversion regime (Fig. 3b), and significant difference in the activation energies was revealed (Table 1). Clearly, conversion efficiencies of chlorinated ethanes were in accordance with their Bond Dissociation Energies (BDEs) of C—Cl (Table 1), and the dissociation of C—Cl bond was crucial and intrinsic for the catalytic oxidation of CVOCs, which was consistent with our DFT calculation results (Fig. S1). However, it can be also found that 1,2-DBE did not give a lower activation energy despite the cleavage of the C—Br bond needs much lower energy than the C—Cl cleavage, which was probably due to the difference between adsorption of Br and Cl on oxygen vacancies or acid sites of CeO_2. Nevertheless, it can be concluded that the dissociation of C—Cl bond was crucial and the first step or the rate-determining step in the catalytic decomposition of CVOCs over CeO_2 based catalysts.

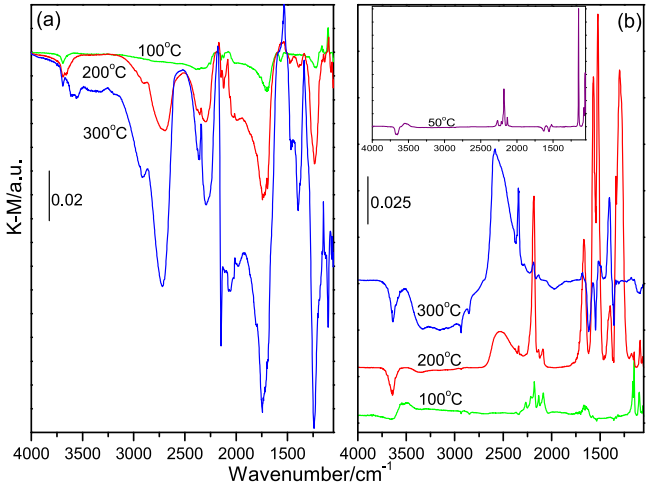

Fig. 5. *In situ* DRIFT spectra of deuterated 1,2-dichloroethane (DDCE) oxidation over pure CeO_2 (a) and $6.0\%VO_x/CeO_2$ (b) catalysts at different temperature.

3.2. The role of H_2O and surface hydroxyl groups

The roles of H_2O and surface hydroxyl groups were investigated *via* isotopic tracer and *in situ* IR techniques due to the impact of water on the behavior of CVOCs oxidation catalysts and the dissociation into surface hydroxyl groups [31–36]. Fig. 4a presented DCE conversion over pure CeO_2 and $6\%VO_x/CeO_2$ catalysts at 250 °C under dry and humid conditions (3% water vapor). The deactivation of pure CeO_2 was very rapid at 250 °C, thus the effect of H_2O on stability was examined separately, not *via* the switching mode of water vapor. It should be noted that the DCE conversion over pure CeO_2 was higher than that over $6\%VO_x/CeO_2$, which was opposite to the results of activity tests (Fig. 1). It was probably because that the deactivation of pure CeO_2 already occurred during activity tests due to the prolonged heating step (90 min was spent from 100 to 250 °C). These results also further confirmed that the CeO_2 was the main active component for catalytic oxidization of CVOCs over CeO_2 based catalysts. As shown in Fig. 4, the presence of water obviously inhibited the oxidation of DCE primarily due to the blockage or competitive adsorption of water molecules on active sites. Moreover, such impact on $6\%VO_x/CeO_2$ was more noticeable than that on pure CeO_2 and the DCE conversion decreased from 95 to 75%. The possible reasons were the decrease of the number of strong Brönsted acid sites at VO_x species [32] and the weak affinity of the pure CeO_2 for water [31]. Fig. 4b illustrated the H_2O-TPD profiles of pure CeO_2 and $6\%VO_x/CeO_2$ catalysts. According to the work of Wang et al. [37], the adsorption of water on ceria surface may involve

Table 2
Absorption bands for adsorption of perdeuterated 1,2-dichloroethane on pure CeO_2 and 6%VO_x/CeO_2.

CeO_2			6%VO_x/CeO_2		
Bands/cm^{-1}	Assignment	Comments	Bands/cm^{-1}	Assignment	Comments
3697, 3649	—OH	Negative bands	3637	—OH	Negative band
2290–2720	—OD	2540 cm^{-1}, broad band, H/D exchange [17]	2290–2700	—OD	2540–2580 cm^{-1},broad band, H/D exchange
2340	CO_2	Adsorbed CO_2	2340	CO_2	Adsorbed CO_2
2180	CO	Max at 300 °C [39]	2183	CO	CO on strong Lewis sites
2138	Acetaldehyde	νsCD_3, intermediate species [40]	2134	Acetaldehyde	νsCD_3, intermediate species
2083	CO	Twin CO [41]	2089	CO	Twin CO
1530	Carboxylate	$\nu s(COO^-)$, strong band, max at 300 °C [42]	1524	Carboxylate	Max at 200 °C
1335	Enolic species	RCH = CH—O—, at 200 and 300 °C [43]	1336	Enolic species	RCH = CH—O—, only at 200 °C
1145	Deuterated 1,2-dichloroethane	δaCD_2 [43]	1176	Deuterated 1,2-dichloroethane	ρCD_2 δaCD_2
1095			1147		
1064			1087		
			1060		
2058	CO	Weak bands, linear, twin and bridged CO molecules adsorbed on $Ce^{3+/4+}$	1668	Acetate/acetic acid [40]	ν(C=O) νa(COO) $\nu s(COO^-)$ νs(CO—O)
2013			1569		
1920			1395		
			1299		
2864	Aliphatic, -CH_3, -CH_2-	H/D exchange of —OH and DDCE			

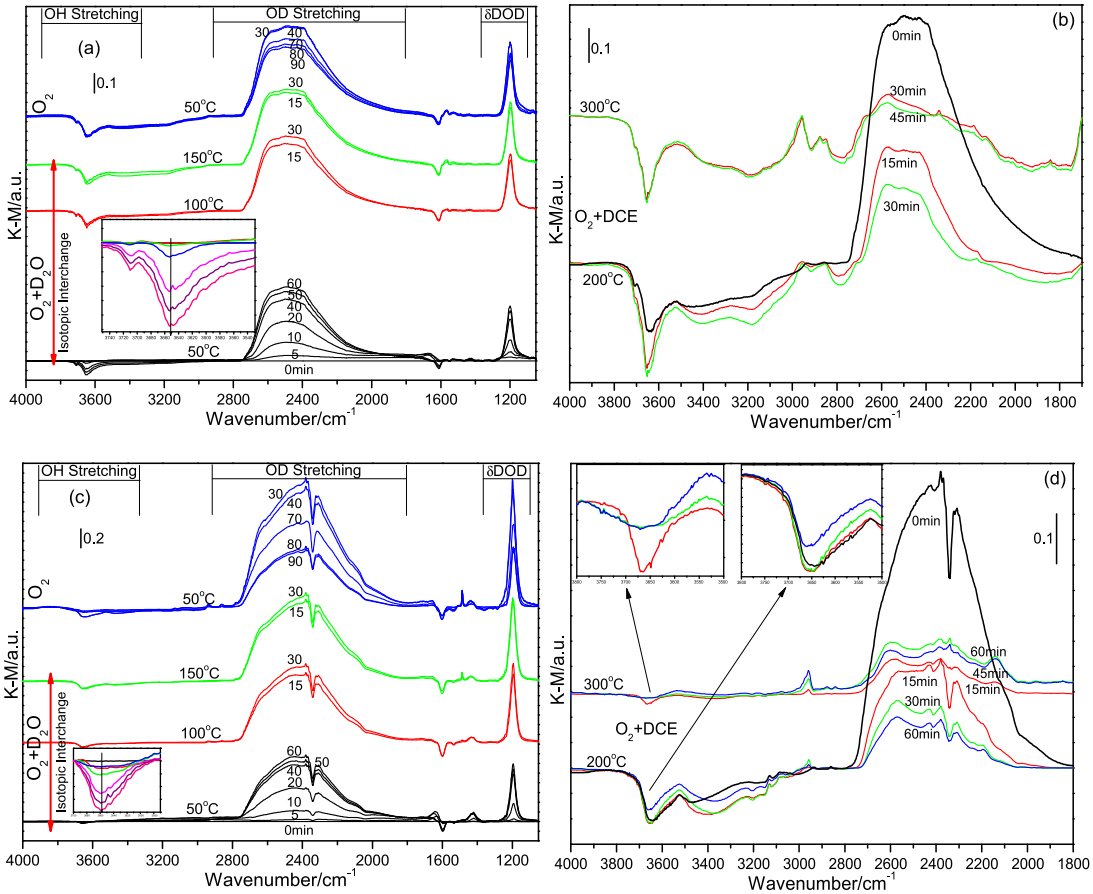

Fig. 6. FTIR spectra during H/D exchange of CeO_2 (a) and 6%VO_x/CeO_2 (c) at different temperature under flowing D_2O/O_2 (50 ml/min, 3 v/v% D_2O vapor), and *in situ* DRIFT spectra of 1,2-dichloroethane (DCE) oxidation over deuterated CeO_2 (b) and 6.0%VO_x/CeO_2 (d).

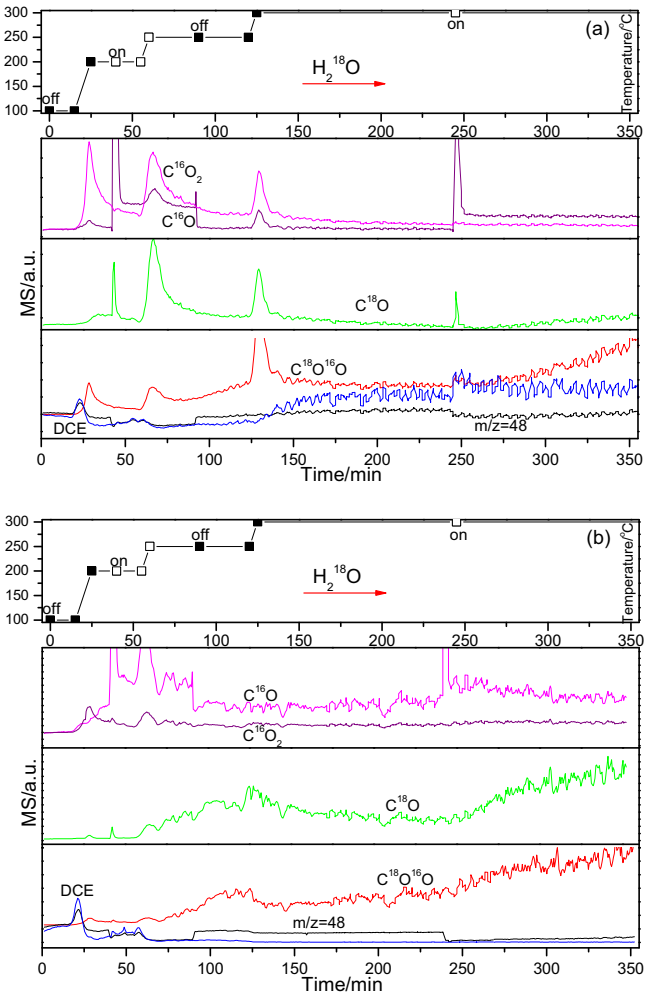

Fig. 7. TPSR profiles of DCE oxidation over pure CeO_2 and 6%VO_x/CeO_2 catalysts under 0.6 v/v% $H_2{}^{18}O$ vapor. Reaction conditions: pretreated for 2 h at 300 °C under 30 ml/min O_2/Ar; 200 mg catalysts, 500 ppm DCE, 0.6%$H_2{}^{18}O$ vapor, 20% O_2, Ar balance, 30 ml/min.

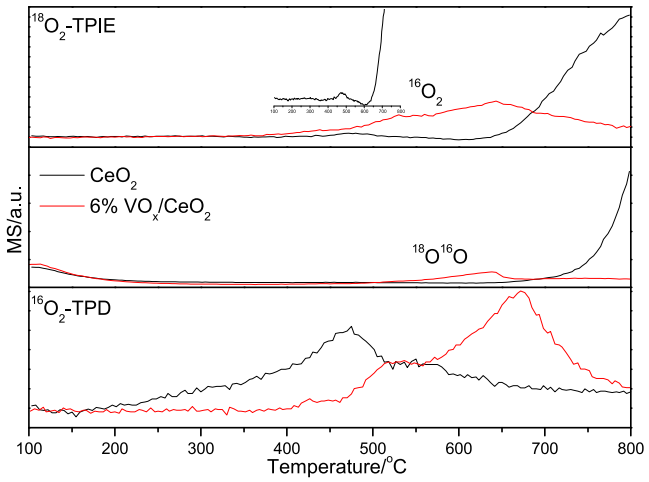

Fig. 8. Temperature-programmed isotopic exchange (TPIE) and $^{16}O_2$-TPD over pure CeO_2 and 6%VO_x/CeO_2 catalysts. TPIE: 5% $^{18}O_2$ in Ar flowing at 30 ml/min, mass of the catalyst 100 mg; $^{16}O_2$-TPD: Ar flow of 30 ml/min, mass of the catalyst 100 mg.

three types: Type-I water molecules are included in the interparticle space and had no interaction with the ceria surface; Type-II water molecules interact with pre-adsorbed water or hydroxyls at the surface through hydrogen bonding; Type-III water molecules are associatively adsorbed on ceria. Among them, Type-III water is most important and may provide protons as acid sites. It can be found that 6%VO_x/CeO_2 exhibited a stronger affinity for water molecule (the desorption temperature was higher and peak width was wider) and the concentration of Type-III water was also higher compared with pure CeO_2. Furthermore, the activity of 6%VO_x/CeO_2 could be fully recovered after the water vapor was switched off and kinetic isotope effect of D_2O (H_2O vapor was replaced by D_2O vapor) was not observed, indicating that the negative effect of water was reversible and water dissociation/activation was not involved in oxidation reaction or the rate limiting step. However, it is generally accepted that water molecule can dissociate into an OH group binding at cerium and an H at a surface oxygen atom, giving rise to a hydroxyl pair (O_sH_{ads}-OH_{ads}) [38], and they can play vital roles in many catalytic reactions [17,35]. Thus, the roles of water and surface hydroxyl group were further investigated by *in situ* FTIR studies of DDCE oxidation and H/D exchange of surface hydroxyl groups *via* D_2O, and TPSR in the presence of $H_2{}^{18}O$.

The adsorption of perdeuterated 1,2-dichloroethane (DDCE) on pure CeO_2 and 6%VO_x/CeO_2 catalysts was studied by situ DRIFT between 50 and 300 °C, and the spectra were shown in Fig. 5 (the C—Cl absorption bands was not observed) and the absorption bands were summarized in Table 2. Moreover, Fig. 5b inset showed the C—D vibration frequency for the physically adsorbed DDCE on 6%VO_x/CeO_2 at 50 °C and a series of bands can be observed at 2265, 2214, 2179, 2132, 1594, 1516, 1150, 1077 and 1056 cm^{-1}, which were shift to lower wavenumber compared to DCE due to the stronger bond of C—D than C—H [15]. As the temperature rose to 100 °C, the number and intensities of bands significantly reduced due to the occurrence of desorption. When the temperatures went up further, numerous bands were observed and the number/intensity varied with catalysts and the temperature. The detailed assignments and comments can be found in Table 2. Based on these formed species, it was speculated that the catalytic oxidation of 1,2-dichloroethane over CeO_2 based catalysts involved the following pathways: enolic species → aldehyde → acetate/acetic acid → CO → CO_2. However, the formation temperature and number of these intermediate species were different, which was mainly related to the differences in redox performance and acid-base properties of catalysts. Additionally, it can be found that a broad band in the 2800–2200 cm^{-1} range (about 2540 cm^{-1}) was observed, which corresponded to the —OD stretching [17] and might come from H/D exchange of —OH and DDCE, the formation of —OD *via* a direct dissociation of DDCE on basic oxygen species or readsorption/dissociation of the formed D_2O on active sites such as oxygen vacancies, O^{2-} or $Ce^{3+/4+}$. However, the first two routes can be negligible because the splitting of C—D bond was very difficult. Nevertheless, the formation of —OD and disappearance of —OH indicated that the surface hydroxyl groups were involved in the oxidation of 1,2-dichloroethane.

The H/D exchange was accomplished by passing an O_2 feed (50 ml/min) through a water saturator thermostatted at 25 °C to produce a 3 v/v% D_2O/O_2 feed. This feed was then contacted with a catalyst (50 mg) placed in the sample cell of *in-situ* IR spectroscopy. The exchange process was followed with IR spectroscopy to monitor the degree of exchange (Fig. 6a and c). Upon contact with the D_2O/O_2 feed, the bands corresponding —OD stretching (2800–1800 cm^{-1}) and δDOD bending (1200 cm^{-1}) bands were detected. Meanwhile, the bands attributed to the surface —OH and adsorbed water on the catalysts quickly disappeared, because two negative bands were observed, the broad band at 3800–3500 cm^{-1} was due to hydrogen-bonded OH stretching arising from surface hydroxyl groups and the δHOH bending vibrations centered at 1600 cm^{-1} were exclusively due to adsorbed water [17]. There-

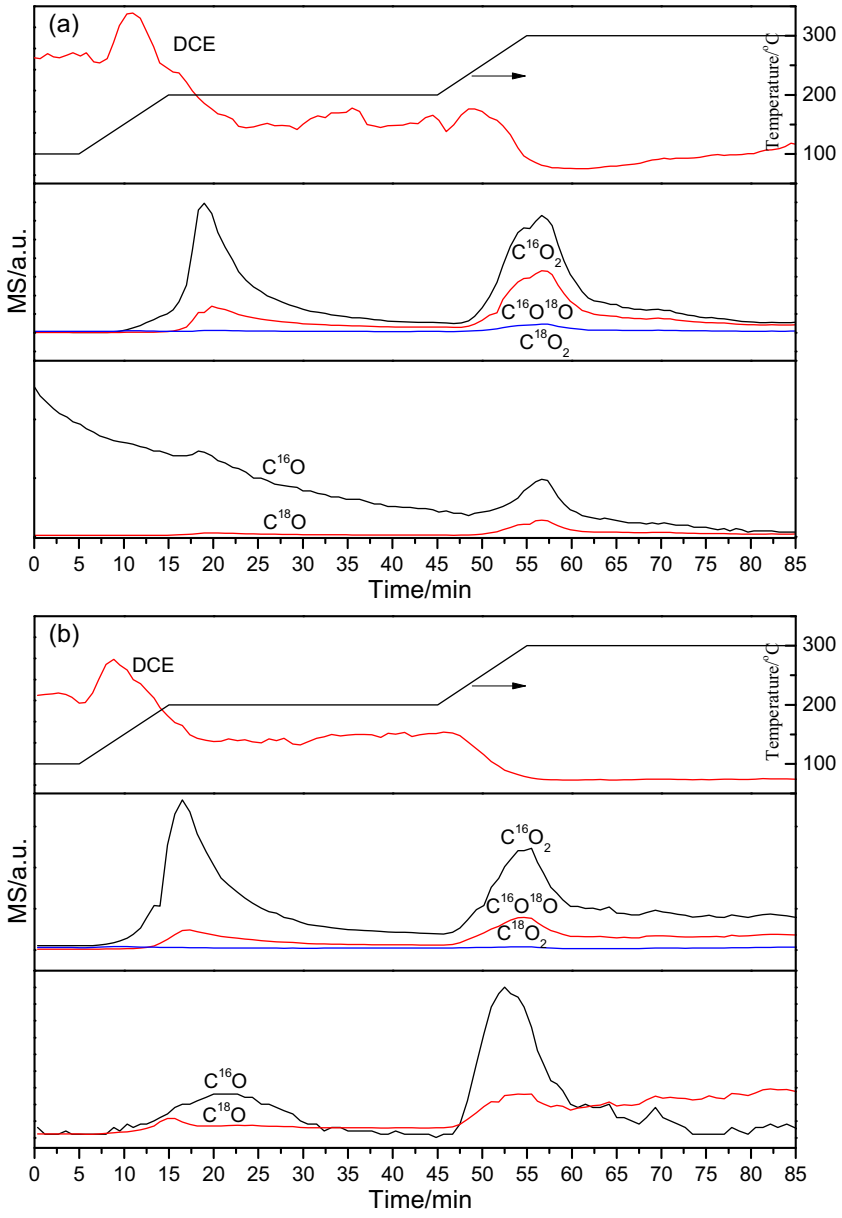

Fig. 9. CO_x species profiles in TPSR of $^{18}O_2$ and 1,2-dichloroethane over pure CeO_2 and 6%VO_x/CeO_2 catalysts. 5% $^{18}O_2$ in Ar flowing at 50 ml/min, 1000 ppm DCE, mass of the catalyst 200 mg.

fore, the H/D exchange was an extremely facile process at 50 °C and largely complete 30 min after the initial contact with D_2O. For purposes of obtaining more surface —OD, the prolonged exchange at higher temperature (100 and 150 °C) were carried out. After the exchange was finished, the D_2O was removed from the gas feed and the catalyst was flushed for additional 90 min with O_2 until no further changes occurred to the spectra. Subsequently, *in situ* DRIFT spectra of DCE oxidation over these catalysts (the —OH was replaced by surface —OD) were obtained at 200 and 300 °C (Fig. 6b and d). Accompanying with the DCE oxidation, the number of surface —OD existing on both catalysts gradually decreased, which was a strong indication that surface —OD was consumed and involved in the DCE oxidation. Simultaneously, the bands corresponding to surface —OH over 6%VO_x/CeO_2 catalyst were gradually recovered and nearly restored to its initial state after the oxidation reaction was maintained for 45 min at 300 °C. However, the increase of surface —OH bands for pure CeO_2 catalyst was almost negligible, which suggested that the surface —OH of pure CeO_2 was not replenished even at 300 °C. Therefore, it can be speculated that difficult replenishment of the consumed surface hydroxyl groups (*via* the formation of HCl) can be one of the main reasons of pure CeO_2 catalyst deactivation. In addition, our DFT calculations indicated that the dissociative configuration of HCl (Fig. S2b) was energetically more favorable than that of molecular adsorption (Fig. S2a) by 0.62 eV. Thus, though the formation of HCl was facile, it would be likely to dissociatively adsorb on CeO_2. Our previous work also suggested that the deactivation of pure CeO_2 due to Cl poisoning could be resolved only through the formation of Cl_2 at higher temperature (Deacon reaction, above 330–350 °C) [14].

Fig. 7 showed TPSR profiles of DCE oxidation over pure CeO_2 and 6%VO_x/CeO_2 catalysts under 0.6 v/v% $H_2{}^{18}O$ vapor, which was used to determine whether the oxygen of surface hydroxyl groups were involved in DCE oxidation. It is generally accepted that the water molecule can dissociate into an OH group binding to Ce or filling an oxygen vacancy and an H binding to a surface oxygen atom. Thus, during TPSR tests, the $H_2{}^{18}O$ molecules on CeO_2 surface can

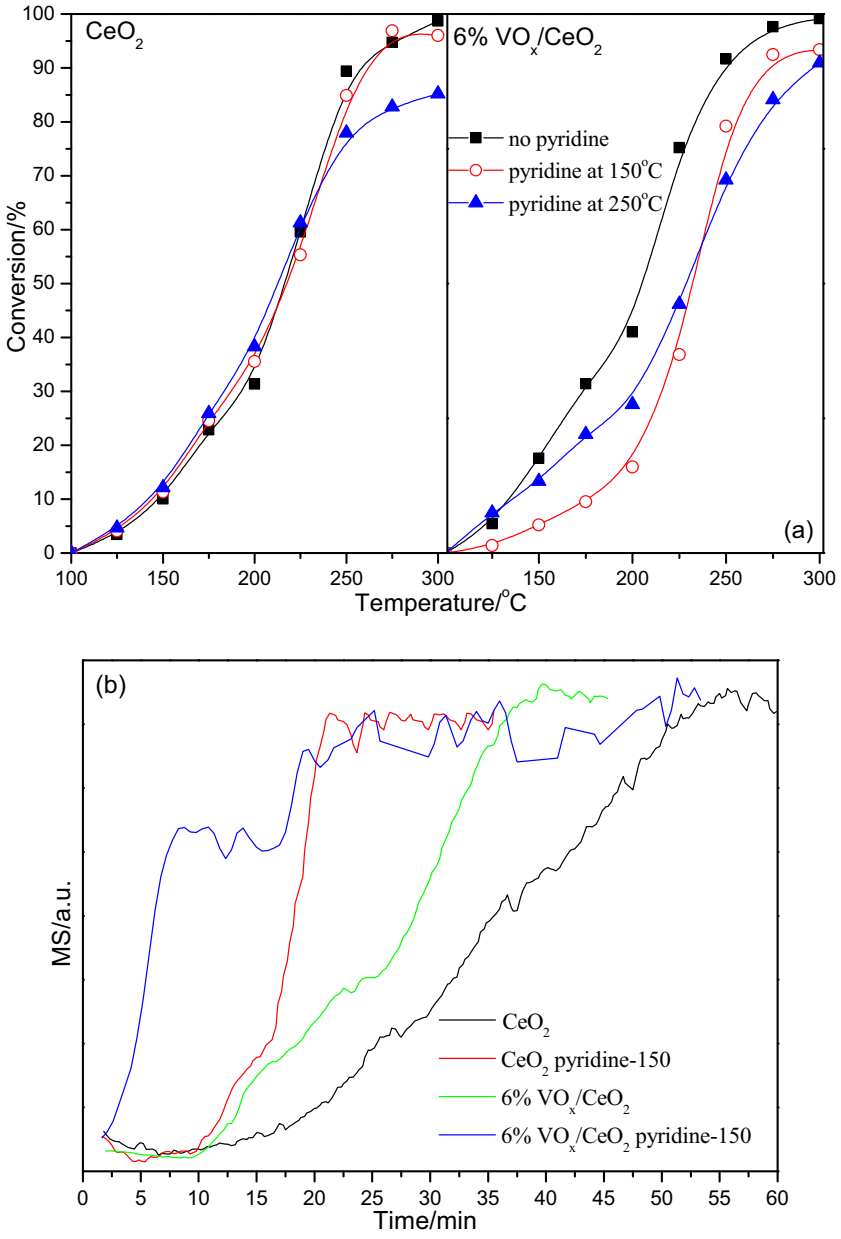

Fig. 10. Conversion curves for DCE oxidation (a) and breakthrough curves of DCE adsorption (b) over CeO_2 and 6%VO_x/CeO_2 adsorbing pyridine at different temperature. Catalysts were pretreated for 1.5 h at 300 °C in O_2 flowing; 200 mg catalysts, 500 ppm DCE, 20% O_2, Ar balance.

evolve to the Ce-^{18}OH or V-^{18}OH (V is an oxygen vacancy) and ^{16}O H. According to the results shown in Fig. 7, $C^{18}O$ and $C^{18}O^{16}O$ both were observed over the two catalysts and their amounts gradually increased or decreased after the $H_2{}^{18}O$ vapor was introduced or switched off, while the formation of $C^{18}O_2$ was negligible. However, it should be noted that $C^{16}O$ and $C^{16}O_2$ were still the main products, especially on pure CeO_2 catalysts, which indicated that the surface adsorbed oxygen or lattice oxygen species from catalysts involved the oxidation reaction. The formation of $C^{18}O$ and $C^{18}O^{16}O$ was considered to originate from further oxidation of the intermediate acetaldehyde owing to the attack of formed $^{18}O^-$ and hydrogen transfer [15].

3.3. The role of gaseous and lattice oxygen

Temperature programmed isotopic exchange (TPIE) over pure CeO_2 and 6%VO_x/CeO_2 catalysts was performed as a function of temperature in order to examine the mobility of surface oxygen or lattice oxygen. Fig. 8 showed that these two catalysts exhibited similar trends: the oxygen exchange was negligible below 350 °C. However, with the steady increase of temperature, a different behavior was observed. 6%VO_x/CeO_2 catalyst showed evident isotopic oxygen exchanges in the 350–800 °C ($^{16}O^{16}O$) and 500–650 °C ($^{16}O^{18}O$) range. Two $^{16}O^{16}O$ peaks were observed at 530 °C and 640 °C, and the former was more likely to be assigned to the desorption of surface oxygen species and $^{16}O_2$-TPD further confirmed the possible desorption. Additionally, a maximum $^{16}O^{18}O$ formation peak appears near 640 °C. The simultaneous evolution of the $^{16}O^{16}O$ and $^{16}O^{18}O$ suggested that reaction mechanisms involving both simple and multiple pathways took place at the same time [44,45]. In the case of pure CeO_2 catalyst, a weak $^{16}O^{16}O$ peak appeared at 470 °C (the desorption of surface oxygen species), but the main evolutions of $^{16}O^{16}O$ and $^{16}O^{18}O$ only occur above 625 °C and 650 °C, respectively. $^{16}O^{16}O$ was the first to be observed in the gas phase, which indicated a multiple heteroexchange with simultaneous participation of two oxygen atoms of the oxide and involvement of

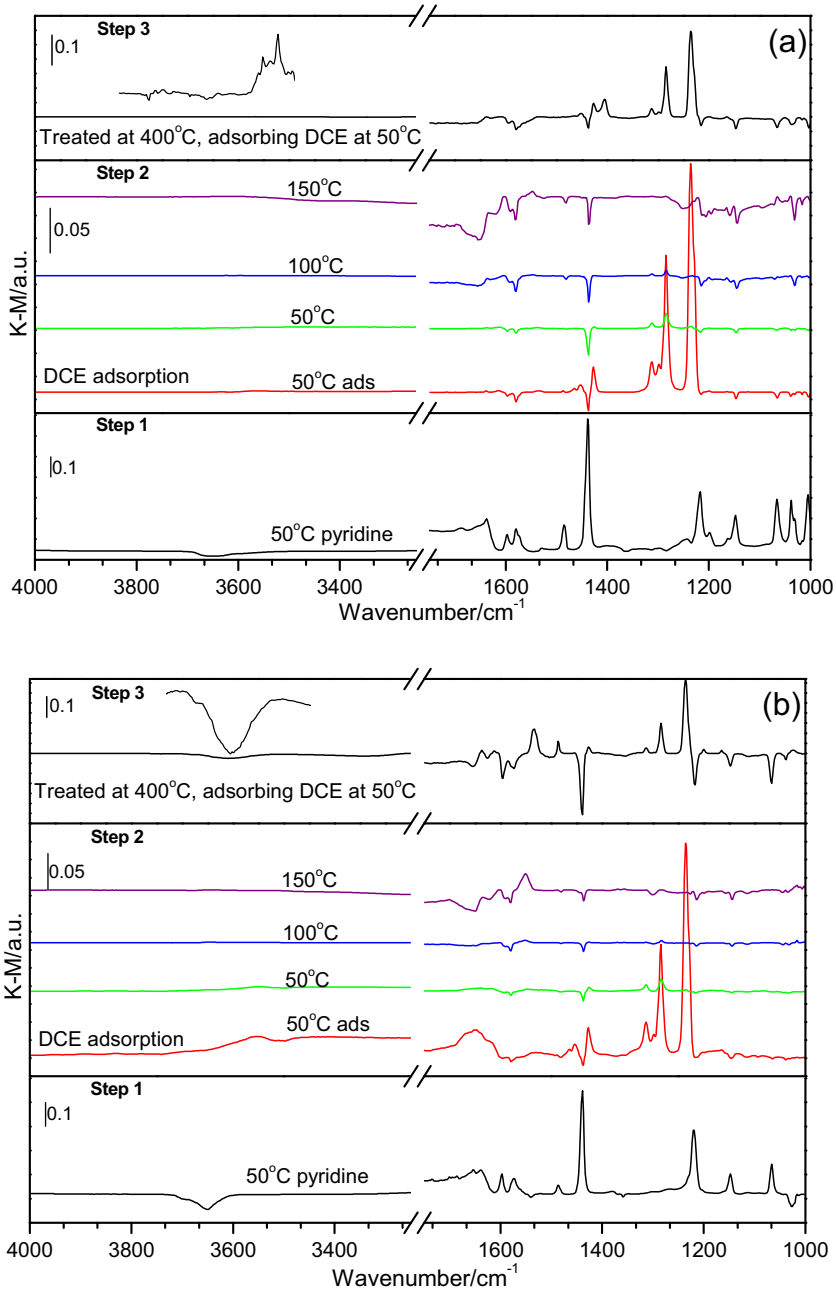

Fig. 11. *In situ* FTIR spectra of DCE oxidation over CeO_2 (a) and 6%VO_x/CeO_2 (b) adsorbing pyridine.

surface dioxygen intermediates such as superoxides (O_2^-) or peroxides (O_2^{2-}) [44]. Additionally, it was evident that the lattice oxygen mobility of 6%VO_x/CeO_2 catalyst was higher than that of pure CeO_2 according to the isotopic exchange temperature, which was ascribed to the strong interaction VO_x and CeO_2.

Fig. 9 demonstrated profiles of CO_x species in TPSR of 1,2-dichloroethane over pure CeO_2 and 6%VO_x/CeO_2 catalysts under 5 v/v% $^{18}O_2$ in Ar flowing. Over both pure CeO_2 and 6%VO_x/CeO_2 catalysts, the CO_2 species containing ^{16}O ($C^{16}O_2$ and $C^{16}O^{18}O$) were detected, while $C^{18}O_2$ was negligible. Moreover, the formation of $C^{16}O_2$ occurred earlier than $C^{16}O^{18}O$ and remained as the predominant one, especially during the first stage of heating process. These results indicated that the oxygen required for CO_2 production came from the combination of the surface lattice oxygen and other surface oxygen species such as adsorbed active oxygen, not gaseous oxygen. Namely, DCE can be attacked by the surface lattice oxygen of catalysts and aldehyde species or CO was formed, and then these intermediates will be further oxidized into CO_2 by the surface oxygen species, which was consistent with our previous results [15]. As shown by $^{16}O_2$-TPD, the catalyst surfaces were mainly covered by ^{16}O species initially. Therefore, $C^{16}O_2$ was formed earlier and became dominant. With these ^{16}O species on catalyst surfaces being consumed by the reaction, the dissociative adsorption of gaseous $^{18}O_2$ oxygen occurred and continuously replenished the surface oxygen species, giving rise to the evolution of $C^{16}O^{18}O$. Additionally, the nearly 90% selectivity of CO_2 over pure CeO_2 can be due to the abundant surface active oxygen species such as superoxides (O_2^-) or peroxides (O_2^{2-}), which was also verified by the TPIE results. Moreover, the TPSR of DCE over the $^8O_2$ labeled catalysts (the pre-reduced catalysts were oxidized by $^{18}O_2$) in $^{16}O_2$/Ar atmosphere further confirms the involvement of the lattice oxygen (Fig. S3). Fig. S4 also showed that the main product was CO in the

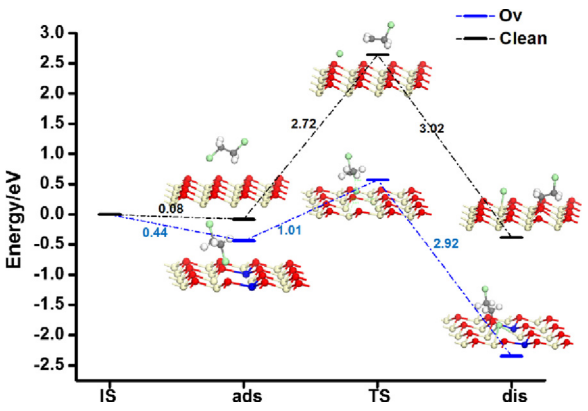

Fig. 12. Calculated energy profile and structures of the key states of the C—Cl cleavage of DCE at (a) clean CeO_2(1 1 1) and (b) reduce CeO_2(1 1 1) (O_v). O is in red, C in gray, H in white, Cl in light green, Ce^{4+} in ivory and Ce^{3+} in blue. (For interpretation of the references to color in this figure legend, the reader is referred to the web version of this article.)

absence of gaseous oxygen even over pure CeO_2 due to the shortage of surface active oxygen. Our previous work indicated that 50–80% selectivity of CO over 6%VO_x/CeO_2 catalyst can be achieved [15], and Fig. 10 also displayed that the main product of the DCE oxidation was still CO ($C^{16}O$ and $C^{18}O$). More importantly, the amount of $C^{18}O$ increased obviously with the increase of reaction temperature and time, which suggested that it was the surface lattice oxygen that participated in the oxidation of DCE to CO, since it can be replenished with oxygen from the gas phase *via* oxygen exchange.

3.4. Selective poisoning and active sites

To obtain further insight into the relationship between surface acid properties of catalysts and their catalytic activity for the DCE oxidation, and understand possible active sites for CVOCs oxidation over CeO_2 based catalysts, we performed additional catalytic tests with pre-adsorption of pyridine (acid poisoning molecule) on catalysts surface at different temperature. Fig. 10a presented the conversion curves for DCE oxidation over CeO_2 and 6%VO_x/CeO_2 with pyridine being pre-adsorbed at 150 °C and 250 °C. The pre-adsorption of pyridine did not change the light-off curves of the pure CeO_2 catalyst, thereby revealing that the presence of pyridine did not inhibit the DCE oxidation. However, the inhibition effect was observed at high temperature range (above 250 °C), especially over the CeO_2 catalyst with pyridine being pre-adsorbed at 250 °C, which might be associated with the decomposition/oxidation of pyridine (new species were detected above 250 °C for the *in situ* FTIR of pyridine adsorption, Fig. S5). In contrast, the pre-adsorption of pyridine caused a significant activity decrease of 6%VO_x/CeO_2 catalyst. Moreover, the degree of inhibition found in the pre-adsorption at 250 °C was weaker than that at 150 °C, especially within the range of low temperature, owing to the desorption of pyridine on weak acid sites. Thus, it can be concluded that the activity of 6%VO_x/CeO_2 catalyst declined due to the occupation of acid sites by pyridine. Additionally, Fig. 10b showed breakthrough curves of DCE adsorption, and the pre-adsorption of pyridine apparently reduced the adsorption of DCE on CeO_2 and 6%VO_x/CeO_2 catalysts. In brief, the role of acid sites was almost negligible for DCE oxidation over pure CeO_2 catalyst and oxygen vacancies might be the only active site, while the catalytic activity of 6%VO_x/CeO_2 catalyst can be attributed to the combined effects of acid sites and oxygen vacancies.

The adsorption behaviors of DCE and pyridine were further investigated via *in situ* FTIR, and the results were presented in Fig. 11. After pyridine was adsorbed on CeO_2 and 6%VO_x/CeO_2 at 50 °C, an absorption band at 1438 cm^{-1} was observed and attributed to pyridine bonded to Lewis acid sites. Additionally, the DRIFT of pyridine adsorption at different temperatures (Fig. S5) demonstrated that the adsorption of pyridine on Lewis acid sites was strong and the complete desorption did not occur even at 350 °C. The acid strength and amount of 6%VO_x/CeO_2 was higher than pure CeO_2 catalyst, which can be attributed to VO_x species. When DCE was subsequently introduced, it was found that the adsorption of DCE on catalysts with adsorbed pyridine decreased significantly, and the intensity of bands at 1428/1403 cm^{-1} (δ_aCH_2), 1312/1285 cm^{-1} (δ_sCH_2), 1233 cm^{-1} (ρCH_2) was much weaker than that of catalysts treated at 400 °C with O_2 (most of pyridine was removed or oxidized), which was a strong indication of the adsorption of DCE on Lewis acid sites. However, the adsorption bands of DCE can be still observed, which was probably due to the partial desorption of pyridine and the adsorption on other adsorption sites such as oxygen vacancies.

To verify the speculation that oxygen vacancies might be the active sites for DCE oxidation over pure CeO_2 catalyst, we carried out first-principles density functional theory calculations corrected by on-site Coulomb interaction (DFT + U). As can be seen from Fig. 12, the adsorption energy of DCE at reduced surface (O_v) was calculated to 0.44 eV, while it was extremely small (only 0.08 eV) over clean surface. As the dissociation of C—Cl bond was crucial for the catalytic oxidation of CVOCs, we further investigated the cleavage of C—Cl of DCE. The barrier for the C—Cl cleavage of DCE at O_v was calculated to be 1.01 eV and the whole process was exothermic by 1.81 eV, with Cl preferably being located at the oxygen vacancy, rather than Ce^{4+} or Ce^{3+} (see Fig. S6). While for the clean surface, the barrier was extremely high (2.72 eV) and the process was less exothermic of ~0.3 eV only. Therefore, it can be concluded that the C—Cl cleavage of DCE at O_v was more preferable than that at clean surface (surface Ce^{4+}) both thermodynamically and kinetically, which was consistent with our previous reports [8] that commercial CeO_2 or CeO_2 calcined at high temperature (800 °C) showed a poor activity for catalytic combustion of trichloroethylene (see Figs. S7 and S8).

The dissociative adsorption energy of the rest fragment of disassociated DCE (after the cleavage of C—Cl bond) on oxygen species, such as surface lattice oxygen and surface adsorbed peroxide species, was then calculated and the results were listed in Fig. 13. The calculation results showed that the configuration with the fragment being adsorbed at lattice oxygen was energetically more preferable than that with the fragment at peroxide species by 0.48 eV. It needed to be noted that lattice oxygen was more abundant at catalyst surfaces compared to peroxide species which may only exist at pre-reduced surfaces. From a thermodynamic point of view, it can be then expected that the disassociated DCE was more preferable to occur. $^{18}O_2$ labeling experiments had confirmed that the surface lattice oxygen was involved directly in the DCE oxidation, *i.e.*, the disassociated DCE was attacked by the surface lattice oxygen species and partially oxidized to aldehyde species or CO, and then was totally oxidized into CO_2 by the surface peroxide species.

3.5. Stability tests

Durability tests for DCE oxidation over 6%VO_x/CeO_2 catalyst at different temperatures were performed (see Fig. 14a). The results showed that 6%VO_x/CeO_2 catalyst presented a better stability whether at evaluated temperature (250 °C) or at lower temperature (150 °C) during the 10 h tests, and the stable conversion was in accordance with the results of activity tests. The excellent stability at lower temperature also showed that 6%VO_x/CeO_2 catalyst was different with from CeO_2 supported RuO_2 catalysts, the latter

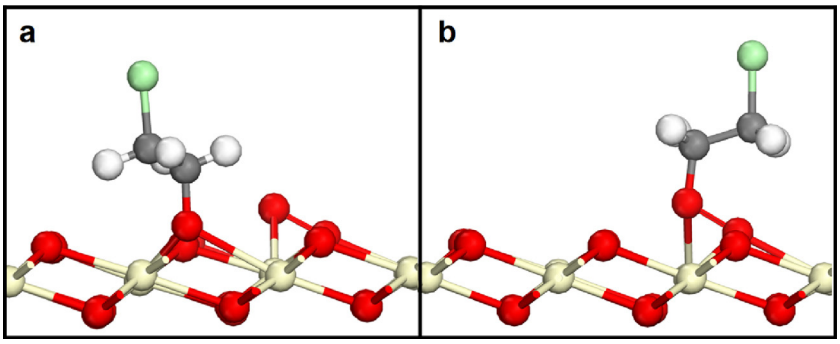

Fig. 13. Calculated structures of the fragment of DCE at (a) lattice oxygen, (b) surface peroxides species.

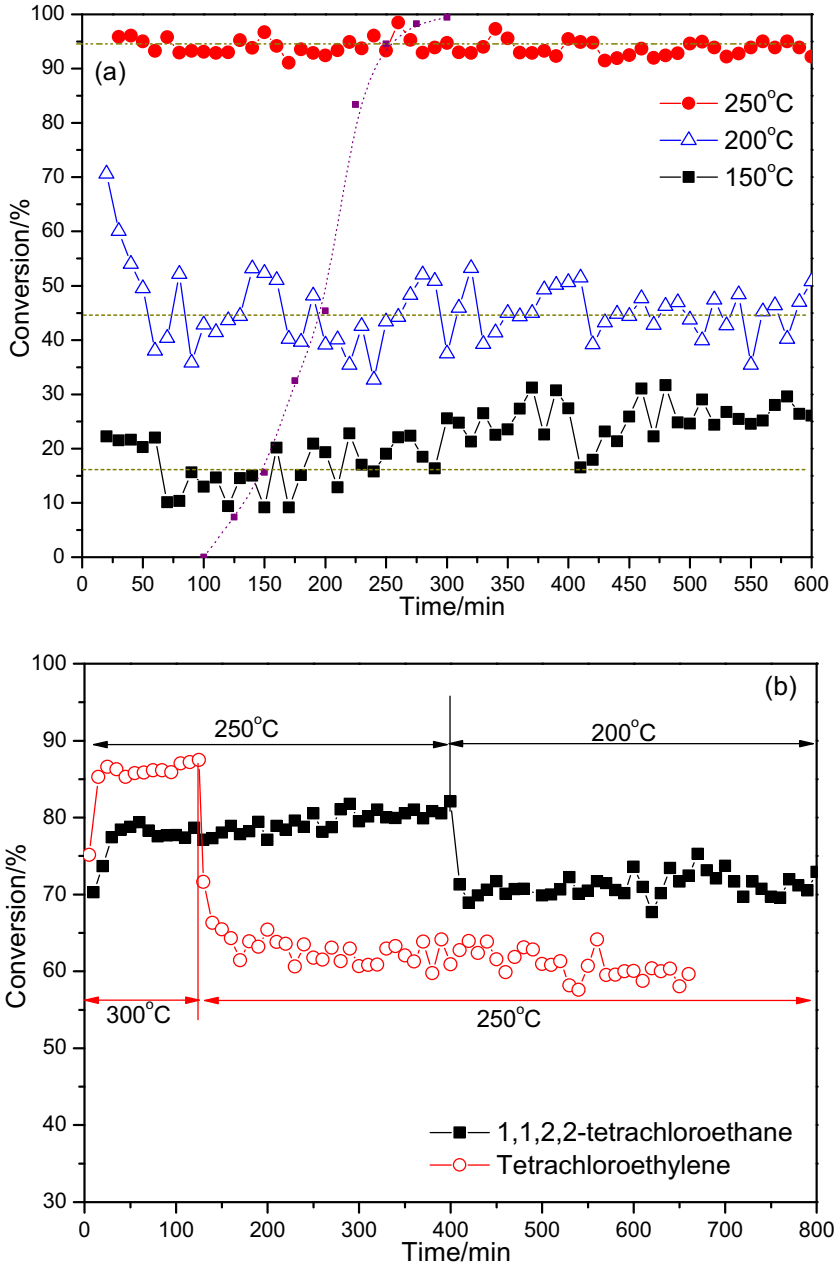

Fig. 14. Durability tests for DCE, 1,1,2,2-tetrachloroethane (TCE) and tetrachloroethylene (PCE) over CeO_2 and 6%VO_x/CeO_2 catalysts at different temperature. Reaction conditions: 200 mg catalysts, 500 ppm CVOCs, 50 ml/min Air.

only achieved a stable activity at higher temperature (above the needed temperature that the adsorbed Cl oxidized into Cl_2), while the stability of the former was attributed to the direct removal of HCl. Additionally, the stability tests of different chlorinated C2 hydrocarbons, including 1,1,2,2-tetrachloroethane (TCE) and tetrachloroethylene (PCE), also were performed to identify whether the 6%VO_x/CeO_2 catalyst was versatile for CVOCs oxidation. Fig. 14b showed that, although only 86% (at 300 °C) and 80% (at 250 °C) conversion of PCE and TCE were achieved, no appreciable deactivation was observed. Subsequently, the reaction temperature was reduced to the lower temperature (PCE at 250 °C and TCE at 200 °C), and the stable conversion could still be maintained. In short, 6%VO_x/CeO_2 catalysts showed an excellent stability for different CVOCs oxidation even at lower temperature, and the deactivation would not occur.

4. Conclusions

Catalytic oxidation of DCE over pure CeO_2 and VO_x/CeO_2 catalysts was systematically investigated *via* isotopic tracer techniques, DFT calculations and selective poisoning of acid sites, and the following results were revealed that: (1) KIEs measurements and activity tests of various halogenated ethanes identify that the activation or dissociation of C—H bond is not a rate determining step and the cleavage of C—Cl bond is the first step for the catalytic combustion of DCE over CeO_2 based catalysts, which is also confirmed by the DFT calculations results that the cleavage of C—Cl bonds is more favorable than the cleavage of C—H and CC both thermodynamically and kinetically. Moreover, VC by-product is formed *via* a abstraction of HCl and determined by the activation of C—H bond, which is the same as the oxidation of DCE over HZSM-5. (2) The presence of water obviously inhibits the oxidation of DCE mainly due to the blockage or competitive adsorption of active sites, but the retarding effect on the strong Brönsted acid sites from VO_x species is still not ignorable for 6%VO_x/CeO_2. *In situ* FTIR of DDCE oxidation and DCE oxidation over D_2O exchanged catalysts demonstrates that surface hydroxyl groups directly react with the adsorbed Cl on oxygen vacancies to form HCl, and the consumed OH could be replenished by the dissociation of water from DCE oxidation. The replenishment of OH is crucial for maintaining a better stability, and the deactivation of pure CeO_2 can be ascribed to the hard recovery of the consumed OH or the easy re-dissociation of HCl. (3) TPSR of $H_2{}^{18}O$ and $^{18}O_2$ with DCE indicates that lattice oxygen is directly involved in oxidation of DCE and formation of intermediate species of partial oxidation such as aldehyde species or CO, and then is totally oxidized into CO_2 by the surface peroxide species. For VO_x/CeO_2 catalyst, CO is the main product due to the high mobility of lattice oxygen and shortage of surface peroxide species. (4) DFT calculations show that the cleavage of DCE at oxygen vacancies is more preferable than that at $Ce^{4+/3+}$ both thermodynamically and kinetically, which indicates that oxygen vacancies are active sites. However, the selective poisoning of acid sites reveals that the presence of strong Lewis acid sites has an obvious promotion effect on the adsorption and activation of DCE on VO_x/CeO_2 catalyst. Additionally, the high reactivity of surface lattice oxygen is also confirmed by DFT calculations.

Acknowledgments

This work was supported by the National Natural Science Foundation of China (Nos. 21307033, 21277047, 21477036, 21322307, 21421004), Shanghai Natural Science Foundation (No. 13ZR1411000), Commission of Science and Technology of Shanghai Municipality (No. 11JC1402900), the National Basic Research Program of China (2011CB808505), the "Shu Guang" project of Shanghai Municipal Education Commission and Shanghai Education Development Foundation (13SG30) for financial support. The authors also thank the National Super Computing Center in Jinan for computing time.

Appendix A. Supplementary data

Supplementary data associated with this article can be found, in the online version, at http://dx.doi.org/10.1016/j.apcatb.2015.10.016.

References

[1] C.E. Hetrick, F. Patcas, M.D. Amiridis, Appl. Catal. B 101 (2011) 622.
[2] Y.J. Guan, C. Li, Chin. J. Catal. 28 (2007) 392.
[3] S. Pitkäaho, T. Nevanperä, L. Matejova, S. Ojala, R.L. Keiski, Appl. Catal. B 138–139 (2013) 33.
[4] Q.Q. Huang, X.M. Xue, R.X. Zhou, J. Mol. Catal. A 331 (2010) 130.
[5] B. de Rivas, C. Sampedro, E.V. Ramos-Fernández, R. López-Fonseca, J. Gascon, M. Makkee, J.I. Gutiérrez-Ortiz, Appl. Catal. A 456 (2013) 96.
[6] B. de Rivas, C. Sampedro, R. López-Fonseca, M. Ángel Gutiérrez-Ortiz, J.I. Gutiérrez-Ortiz, Appl. Catal. A 417–418 (2012) 93.
[7] P. Yang, X.M. Xue, Z.H. Meng, R.X. Zhou, Chem. Eng. J. 234 (2013) 203.
[8] Q.G. Dai, X.Y. Wang, G.Z. Lu, Appl. Catal. B 81 (2008) 192.
[9] B. de Rivas, R. López-Fonseca, J.R. González-Velasco, J.I. Gutiérrez-Ortiz, J. Mol. Catal. A 278 (2007) 181.
[10] H.F. Li, G.Z. Lu, Q.G. Dai, Y.Q. Wang, Y. Guo, Y.L. Guo, Appl. Catal. B 102 (2011) 475.
[11] P. Yang, S.S. Yang, Z.N. Shi, Z.H. Meng, R.X. Zhou, Appl. Catal. B 162 (2015) 227.
[12] P. Yang, Z.H. Meng, S.S. Yang, Z.N. Shi, R.X. Zhou, J. Mol. Catal. A 393 (2014) 75.
[13] Q.G. Dai, S.X. Bai, Z.Y. Wang, X.Y. Wang, G.Z. Lu, Appl. Catal. B 126 (2012) 64.
[14] Q.G. Dai, S.X. Bai, J.W. Wang, M. Li, X.Y. Wang, G.Z. Lu, Appl. Catal. B 142–143 (2013) 222.
[15] Q.G. Dai, S.X. Bai, H. Li, W. Liu, X.Y. Wang, G.Z. Lu, Appl. Catal. B 168–169 (2015) 141.
[16] Q.G. Dai, S.X. Bai, H. Li, W. Liu, X.Y. Wang, G.Z. Lu, CrystEngComm 16 (2014) 9817.
[17] J. Saavedra, H.A. Doan, C.J. Pursell, L.C. Grabow, B.D. Chandler, Science 345 (2014) 1599.
[18] J. Au-Yeung, A.T. Bell, E. Iglesia, J. Catal. 185 (1999) 213.
[19] V.D. Makwana, Y.C. Son, A.R. Howell, S.L. Suib, J. Catal. 210 (2002) 46.
[20] G. Kresse, J. Hafner, Phys. Rev. B 47 (1993) 558.
[21] G. Kresse, J. Hafner, Phys. Rev. B 49 (1994) 14251.
[22] J.P. Perdew, Y. Wang, Phys. Rev. B 45 (1992) 13244.
[23] P.E. Blöchl, Phys. Rev. B 50 (1994) 17953.
[24] G. Kresse, D. Joubert, Phys. Rev. B 59 (1999) 1758.
[25] M. Nolan, S. Grigoleit, D. Sayle, S.C. Parker, G.W. Watson, Surf. Sci. 576 (2005) 217.
[26] M. Nolan, S.C. Parker, G.W. Watson, Surf. Sci. 595 (2005) 223.
[27] A. Alavi, P. Hu, T. Deutsch, P.L. Silvestrelli, J. Hutter, Phys. Rev. Lett. 80 (1998) 3650.
[28] R.W. van den Brink, V. de Jong, R. Louw, P. Magg, P. Mulder, Catal. Lett. 71 (2001) 15.
[29] R. López-Fonseca, A. Aranzabal, J.I. Gutiérrez-Ortiz, J.I. Alvarez-Uriarte, J.R. González-Velasco, Appl. Catal. B 30 (2001) 303.
[30] R. López-Fonseca, A. Aranzabal, P. Steltenpohl, J.I. Gutiérrez-Ortiz, J.R. González-Velasco, Catal. Today 62 (2000) 367.
[31] B. de Rivas, R. López-Fonseca, M.A. Gutiérrez-Ortiz, J.I. Gutiérrez-Ortiz, Chemosphere 75 (2009) 1356.
[32] F. Bertinchamps, A. Attianese, M.M. Mestdagh, E.M. Gaigneaux, Catal. Today 112 (2006) 165.
[33] R. López-Fonseca, J.I. Gutiérrez-Ortiz, M.A. Gutiérrez-Ortiz, J.R. González-Velasco, Catal. Today 107–108 (2005) 200.
[34] M.E. Swanson, H.L. Greene, S. Qutubuddin, Appl. Catal. B 52 (2004) 91.
[35] T. Fujitani, I. Nakamura, M. Haruta, Catal. Lett. 144 (2014) 1475.
[36] C.K. Costello, J.H. Yang, H.Y. Law, Y. Wang, J.N. Linc, L.D. Marks, M.C. Kung, H.H. Kung, Appl. Catal. A 243 (2003) 15.
[37] Y.H. Wang, F. Wang, Q. Song, Q. Xin, S.T. Xu, J. Xu, J. Am. Chem. Soc. 135 (2013) 1506.
[38] D. Fernández-Torre, K. Kośmider, J. Carrasco, M.V. Ganduglia-Pirovano, R. Pérez, J. Phys. Chem. C 116 (2012) 13584.
[39] C. Volkringer, H. Leclerc, J.C. Lavalley, T. Loiseau, G. Ferey, M. Daturi, A. Vimont, J. Phys. Chem. C 116 (2012) 5710.
[40] M.R. Manon, F.J. Jeurissen, J.J. Jorna, B.E. Nieuwenhuys, G. Sinquin, C. Petit, J.P. Hindermann, Catal. Today 54 (1999) 65.
[41] X.Z. Jiang, Y.H. Su, B.J. Lee, S.H. Chien, Appl. Catal. A 211 (2001) 47.
[42] K. Saikia, D. Sen, S. Mazumder, P. Deb, RSC Adv. 5 (2015) 694.
[43] Q. Wu, Y.B. Yu, H. He, Chin. J. Catal. 27 (2006) 993.
[44] Y. Madier, C. Descorme, A.M. Le Govic, D. Duprez, J. Phys. Chem. B 103 (1999) 10999.
[45] C. Doornkamp, M. Clement, X. Gao, G. Deo, I.E. Wachs, V. Ponec, J. Catal. 185 (1999) 415.